condensed matter

MDPI

*Article*

# Characterization of Some Physical and Photocatalytic Properties of CuO Nanofilms Synthesized by a Gentle Chemical Technique

**Soumia Aroussi [1], Mohamed Amine Dahamni [1], Mostefa Ghamnia [1,*], Didier Tonneau [2] and Carole Fauquet [2]**

[1] Laboratoire LSMC, Université Oran 1 Ahmed Ben Bella, Oran 31100, Algeria; aroussisoumia@outlook.com (S.A.); pr.dahamni@gmail.com (M.A.D.)
[2] CINaM, CNRS, Aix Marseille Université, 13288 Marseille, France; didier.tonneau@univ-amu.fr (D.T.); carole.fauquet@univ-amu.fr (C.F.)
* Correspondence: mghamnia@yahoo.fr

**Abstract:** Pure and Li-doped CuO nanofilms were synthesized on heated glass substrates using the spray-pyrolysis technique. The deposited pure CuO nanofilms were achieved at a precursor molarity of 0.2 M using a solution prepared from copper nitrate trihydrate ($Cu(NO_3)_2{\cdot}3H_2O$). Doped Li–CuO nanofilms were obtained using several doping concentrations (3, 6, 9, 12 and 15%) by adding a solution prepared from lithium nitrate ($LiNO_3$). The pure and Li–CuO samples were investigated by different techniques. XRD revealed three dominant peaks (-111), (111) and (211), which are the properties of monoclinic CuO. The increase in Li-doping concentration showed the appearance of other peaks of low intensities detected at 2θ ranging from 49 to 68°. AFM images showed a textured and inhomogeneous surface composed of spherical grains whose size decreased with increasing Li doping. UV–visible spectroscopy showed that the CuO samples were of low transparency; the transmittance was less than 50%. The band-gap energy determined from Tauc's equation plot increased from 2.157 to 3.728 eV with the increase in Li doping. These values correspond well to the band gap of semiconducting CuO. The photocatalytic properties were accelerated by Li doping, as revealed by the discoloration of aqueous methylene-blue (MB) solution under ultraviolet irradiation.

**Keywords:** spray pyrolysis; CuO nanofilms; Li doping; optical properties; photocatalytic properties



**Citation:** Aroussi, S.; Dahamni, M.A.; Ghamnia, M.; Tonneau, D.; Fauquet, C. Characterization of Some Physical and Photocatalytic Properties of CuO Nanofilms Synthesized by a Gentle Chemical Technique. *Condens. Matter* **2022**, *7*, 37. https://doi.org/10.3390/condmat7020037

Academic Editor: Víctor Manuel García Suárez

Received: 17 April 2022
Accepted: 23 May 2022
Published: 25 May 2022



## 1. Introduction

Transparent conducting oxides (TCOs) or transition-metal oxides such as ZnO, $SnO_2$, $In_20_3$, etc., have numerous applications and concern various technological areas including microelectronics, photovoltaic energy, biotechnology, batteries, gas sensing, etc. [1–5]. Copper oxide (CuO) is among these TCO materials and has intrinsic interesting chemical and physical properties such as physicochemical properties, photochemical stabilities, electrochemical activity, thermal stability, high thermal conductivity, and so on [6–8]. In addition to these properties, CuO shows interesting photocatalytic activity for photocatalysis applications [9–11].

Copper oxide is an inorganic compound with the formula CuO. It presents as blackish powder and crystallizes in the monoclinic structure with the lattice constants $a$ = 4.6837 Å, $b$ = 3.4226 Å, and $c$ = 5.1288 Å, and β = 99.54° (Figure 1). CuO is a p-type semiconductor with a narrow band gap ranging between 1.2 and 1.8 eV [12–14] and exhibits important physical properties.

Copper oxide can be synthesized by different methods, which can be physical methods such as atomic layer deposition [15], co-precipitation [16], sputtering [17], and Molecular Beam Epitaxy [18], or chemical methods such as chemical vapor deposition [19], spray pyrolysis, spin coating, and sol-gel [20–22]. It has been shown earlier [23] that, amongst these techniques, spray pyrolysis presents many advantages: it is cheaper and easy to implement, while allowing the obtention of homogeneous coatings on large areas. With this method, we can easily obtain nanoscale thin films of good quality.

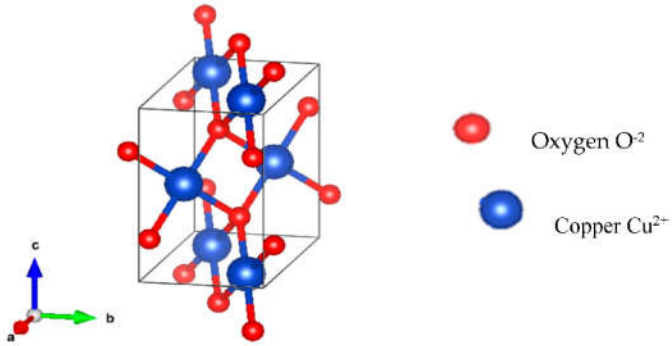


**Figure 1.** Monoclinic structure of CuO.

Nowadays, with the proliferation of industries, the production of pollutant gas has increased, the discharge of wastewater, in particular by the textile industry, is increasing, and human health and nature are threatened. To face this danger, many researchers are studying the photocatalytic properties of metallic nanoparticles [24,25]. It is in this context that we synthesized the oxide CuO using spray pyrolysis, after which we studied the catalytic properties of undoped and Li-doped CuO by monitoring the evolution of the absorption intensity of the solution of methylene blue subjected to UV irradiation.

## 2. Experimental Procedure

In this work, pure and Li-doped copper-oxide nanometric films were deposited onto heated glass substrates using the spray-pyrolysis technique. The primary solution that yields pure copper oxide was prepared by the use of the precursor copper nitrate trihydrate ($Cu(NO_3)_2 \cdot 3H_2O$) in 100 mL deionized water. A secondary solution prepared from lithium nitrate $LiNO_3$ for the Li doping was added to the primary solution at various concentrations ((Li/Cu) ratio: 3, 9, 12 and 15%). These solutions were sprayed onto heated glass substrates maintained at 350 °C during the entire deposition time according to the schema of Figure 2. The obtained pure and Li-doped CuO samples were characterized by techniques adapted to thin-film analysis. X-ray diffraction (XRD-X'Pert PRO from PANalytical utilizing copper line of wavelength $\lambda = 1.54$ Å) was used for structural study. Microstructural and morphological characterizations were obtained by scanning electron microscopy (SEM JEOL 7500-F Instrument) and atomic force microscopy (AFM-Dimension Edge from Bruker), respectively. The CuO band-gap energy (Eg) was graphically estimated using the Tauc's plot, which combines absorption and transmittance data extracted from UV–visible analysis using a Specord 50 plus spectrophotometer. Photocatalytic properties were investigated in a dark chamber where we placed beakers containing the methylene-blue (MB) solution + CuO samples. The whole chamber was illuminated by UV lamp of wavelength 253.7 nm. The absorption of MB solution was measured as a function of Li doping and of UV-irradiation time.

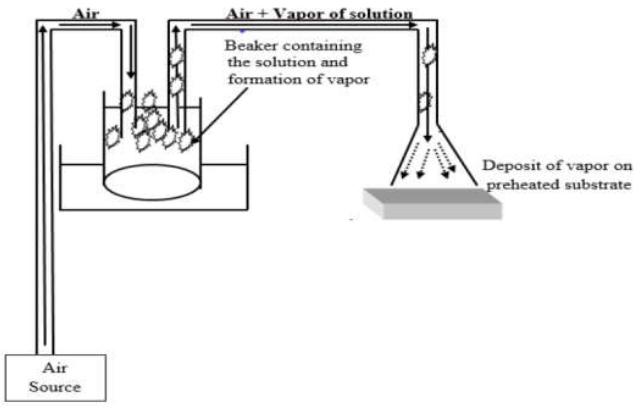


**Figure 2.** Principe schema of spray-pyrolysis technique.

## 3. Results and Discussion

### *3.1. XRD Analysis*

Figure 3 shows the XRD patterns of the deposited pure and Li-doped CuO thin films. More than ten peaks of different intensities were observed with the principal (-111) and (111), (211) indexed planes, corresponding to 2θ diffraction angles around 36 and 38°. The growth of CuO crystals is along these planes, as has been reported by different authors. The observation of more than one peak shows that the copper-oxide films prepared with different Li-doping concentrations were composed of different polycrystalline phases. These peaks are the most frequently shown and discussed in the literature [26,27] and are matched with the JCPDS cards 001–1117 [28], confirming the presence of the monoclinic CuO phase. No impurity peaks were detected, which means that the CuO films were of good quality. When Li doping increased, less intense peaks were observed in the diffraction-angle range of 49–68°, corresponding to (-202), (020), (202), (-113), (022), (220), respectively. This suggests that beyond 9% Li doping, Li atoms had effectively substituted the Cu sites within the CuO lattice. This is favored by the size of $Li^{+}$ which is equivalent to the size of $Cu^{2+}$ ($r_{Li+}$ = 0.76 Å, $r_{Cu2+}$ = 0.73 Å). This explains why the crystal structure is not disturbed much.

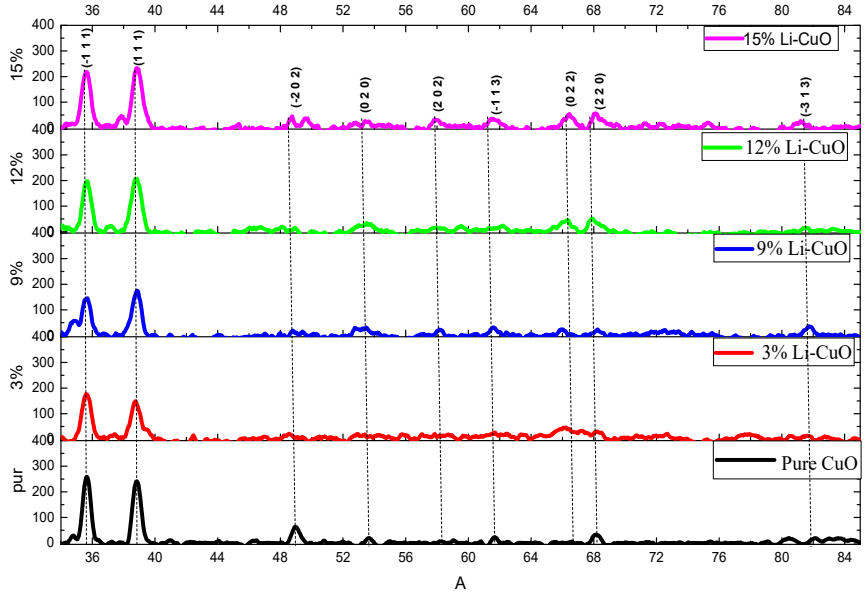


**Figure 3.** XRD spectra of CuO films synthesized by spray-pyrolysis technique.

The exploitation of the major diffraction peaks (-111) and (111) allowed for the determination of the lattice parameters of the monoclinic crystal lattice and the unit-cell volume according to the following relations:

$$\frac{1}{d^2} = \frac{1}{(sin\beta)^2}\left(\frac{h^2}{a^2} + \frac{k^2(sin\beta)^2}{b^2} + \frac{l^2}{c^2} - \frac{2klcos\beta}{ac}\right) \quad (1)$$

$$V = abc\sin\beta \quad (2)$$

where $a$, $b$, $c$ and $\beta$ are the lattice parameters for the monoclinic structure, ($h$, $k$, $l$) are the Miller indices, and $d$ is the interplanar distance.

The lattice parameters $a$, $b$, $c$ calculated from Equation (1) are summarized in Table 1:

**Table 1.** Determination of lattice constants from XRD-spectra processing.

| Sample | *a* (Å) | *b* (Å) | *c* (Å) | *d* (Å) | *β* (°) | *V* (Å)$^3$ |
|---|---|---|---|---|---|---|
| Pure CuO | 4.8808 | 3.4206 | 4.9149 | 2.3164 | 101.618 | 82.0555 |
| 3% Li–CuO doped | 4.9152 | 3.4218 | 5.0335 | 2.3198 | 101.956 | 84.6575 |
| 9%-CuO doped | 4.9449 | 3.4252 | 5.1345 | 2.3265 | 102.361 | 86.9644 |
| 12%-CuO doped | 4.9658 | 3.4277 | 5.2545 | 2.3383 | 102.362 | 89.4382 |
| 15%-CuO doped | 4.9698 | 3.4302 | 5.2837 | 2.3443 | 102.363 | 90.0812 |

From this table, the lattice parameters and the unit-cell volume increase with the increase in Li doping. As $r_{Li^+}$ is greater than $r_{Cu^{2+}}$ ($\frac{rLi^+}{rCu^{2+}} > 1.041$), high Li doping probably distorted the structure by creating defects (essentially point defects as oxygen vacancies), and by increasing the lattice parameters, which explain the increase in unit-cell volume.

We can also estimate, from XRD peak widths, the variation in the average grain sizes of CuO and doped Li–CuO by using the Debye–Scherrer equation [29]:

$$D = \frac{0.9\lambda}{\Delta(2\theta)cos\theta} \quad (3)$$

where $D$ is the mean crystallite size, $\lambda$ is the wavelength of X-ray radiation, $\Delta(2\theta)$ is the angular full width half maximum (FWHM) of the diffraction peaks according to $2\theta$, $\theta$ is Bragg's angle of the peaks.

In order to investigate the influence of Li doping on the structural lattice properties, the dislocation density ($\delta$) [30] was estimated by the use of the following relation:

$$\delta = \frac{1}{D^2} \quad (4)$$

We applied these relations to the most intense diffraction peak (111). The values of $D$ and $\delta$ are shown in Table 2:

**Table 2.** Estimation of the grain sizes and dislocation density of CuO deposits.

| Sample | Δ(2*θ*) (°) | *D* (nm) | *δ*(10$^{-3}$) nm$^2$ |
|---|---|---|---|
| Pure CuO | 0.44702 | 18.6708 | 2.8686 |
| 3% Li–CuO | 0.66885 | 13.3123 | 5.6427 |
| 9% Li–CuO | 0.95583 | 12.2972 | 11.5688 |
| 12% Li–CuO | 0.63674 | 11.9681 | 5.1253 |
| 15% Li–CuO | 0.61111 | 11.1749 | 4.9769 |

From this table, the crystallite size of pure CuO is found be 18.6708 nm and decreases to 11.1749 nm with the increasing in Li doping. This behavior is due to the Li-doping effect, which contributes to the increasing CuO lattice disorder by increasing the Li atoms in CuO films. The surface roughness is clearly affected by the presence of Li atoms as shown in the following paragraph on SEM and AFM images, and similar results have been reported by other authors [31–33].

### *3.2. SEM and AFM Analysis*

The SEM images in Figure 4 are unfortunately blurry; for this reason we have only presented images of the pure and 6% Li-doped CuO. These images show a homogeneous CuO surface composed of granular structures that are clearer in the Li-doped sample. The grains are spherical in shape and uniformly distributed along the surface, resulting in a rough surface.

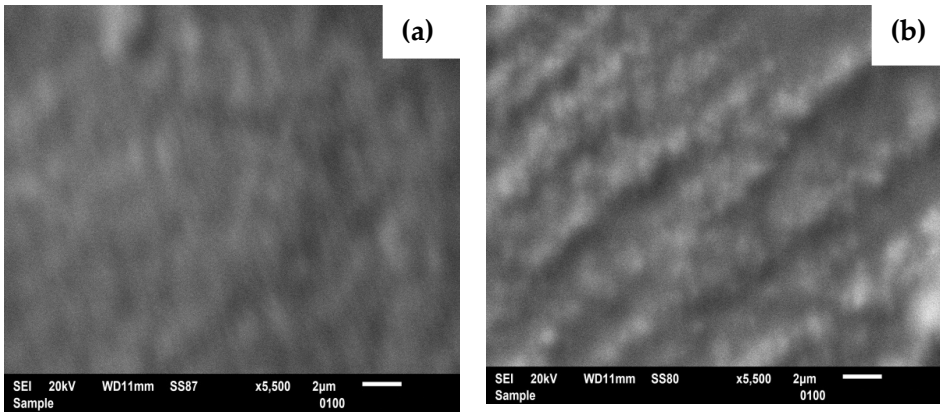


**Figure 4.** SEM images of CuO films. (**a**) Undoped CuO film, (**b**) 6% Li–CuO.

For the surface morphology, we characterized the pure CuO sample and the samples doped with lithium at 3, 6 and 12% by AFM microscopy. AFM images are embedded in Figure 5. The AFM image corresponding to the pure CuO films shows that the surface is composed of islands containing dense spherical CuO grains that are agglomerated and organized in flocks with high porosity, as indicated by voids (dark areas) of irregular shapes. The average flock size was estimated from the profile (Figure 5b,e,h,k) and varied from 20 to 90 nm. The obtained AFM images of CuO films doped with lithium are different from the AFM images of pure CuO. The size of the CuO particles, organized in flocks, increased with the increase in Li doping and become increasingly separated by a great void. The surface roughness, expressed by rms (root mean square), decreased from 48 to 30 nm when Li doping increased from 3 to 12% (Figure 5c,f,i,l).

### *3.3. Optical Properties*

The transmittance T and absorbance α were used for defining the optical properties of CuO. T and α were determined for our samples by using UV–visible spectrometry with a double-beam spectrophotometer operated in the wavelength range 200–900 nm. As our CuO-deposit films were pale in color tending towards dark, the spectra of the transmittance signals that we recorded were very low, not exceeding 50% for all samples, which is in agreement with other works [34,35]. In contrast, the absorbance spectra were intense. This allows us to conclude that the CuO films were not very transparent. This is attributed to the inhomogeneity of the surface as observed in the AFM images.

By combining the transmittance and absorption data and applying Tauc's relation [36]:

$$(\alpha h\nu)^2 = A(h\nu - E_g) \quad (5)$$

where α is the absorption yield, hν is the photon energy, A is a constant, $E_g$ is the band-gap energy, we determined the values of the band gap $E_g$ of CuO from the plot of Equation (5) by extrapolation the linear portion of the curve to $(\alpha h\nu)^2 = 0$, which intersects the energy axis (Figure 6).

The intersection shown by dashed lines gives the approximate value of the band-gap energy. These values are summarized in Table 3. It was observed that Eg was sensitive to Li doping. The band-gap values of the deposited CuO films, shown in Table 3, varied from 2.1722 eV for pure CuO to 3.5608 eV for 15% Li–CuO. The increase in the gap may be due to the formation of Cu–Li–O nanocrystallites at higher doping concentrations by introducing some defects and disorder due to the substrate temperature, which reduce the size of CuO nanocrystallites. It is admitted that the gap of nanostructured systems is greater than the gap of the bulk materials [37–39]. According to the AFM images, which showed discontinued CuO deposits composed of different areas and according to the obtained Eg values, we can conclude that the areas where CuO was deposited were nanostructured.

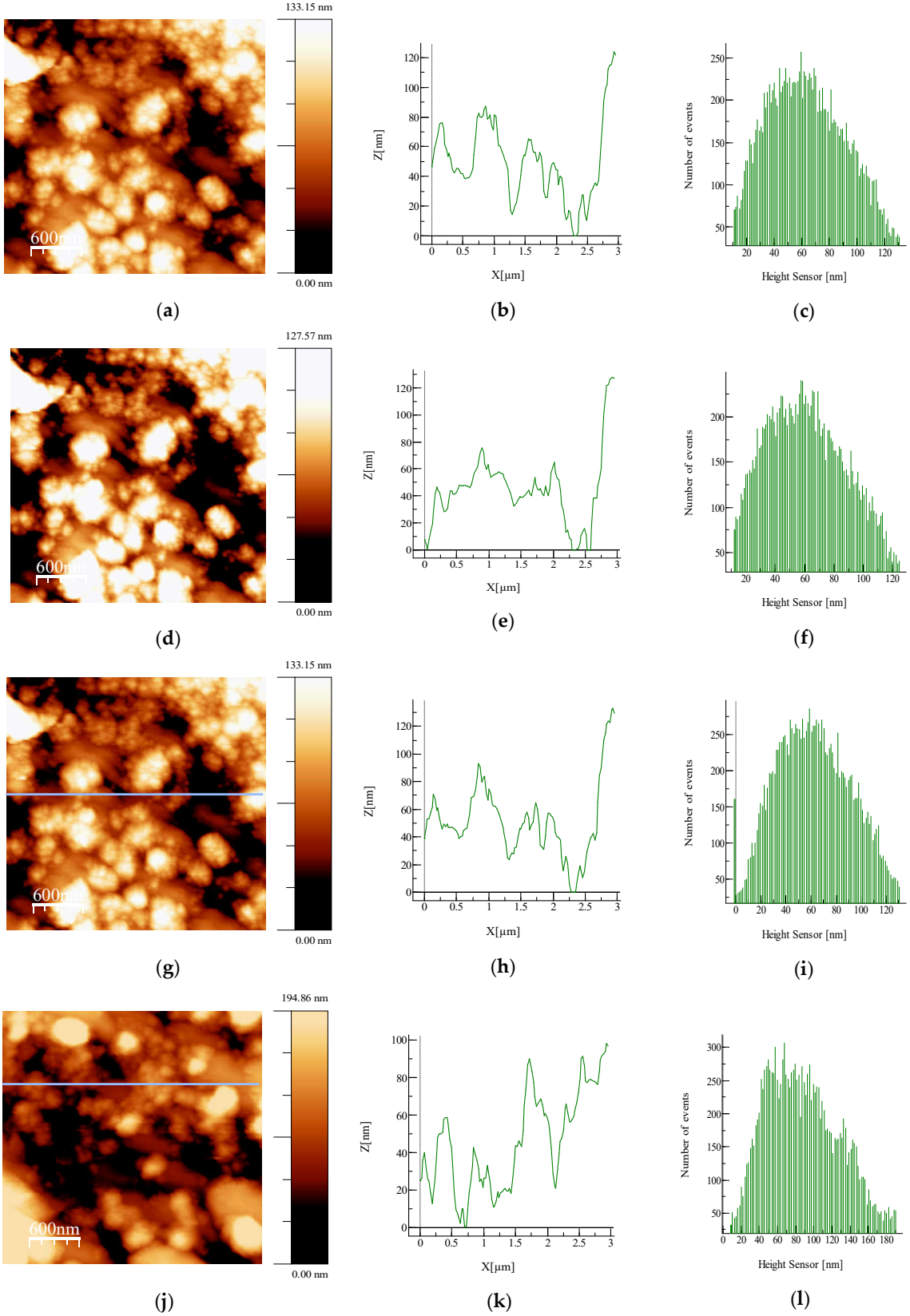


**Figure 5.** AFM images of pure (**a**) to 12% doped Li–CuO (**j**). (**b**,**e**,**h**,**k**) are the profiles of the surface morphology along the horizontal lines drawn on the images (**a**,**d**,**g**,**j**) and (**c**,**f**,**i**,**l**) are the roughness profiles of whole the surface.

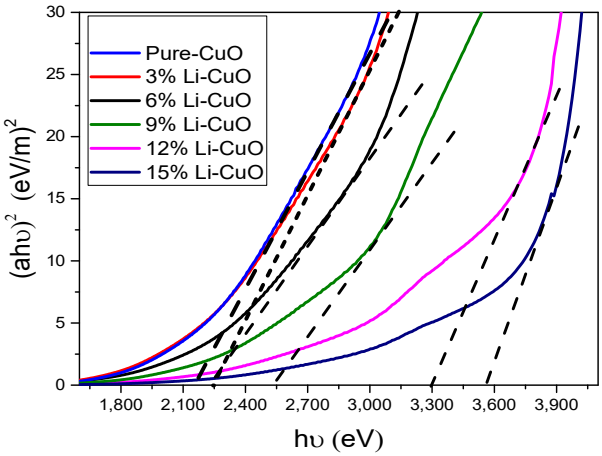


**Figure 6.** Plot of $(\alpha h\nu)^2$ vs. $h\nu$ for pure and Li-doped CuO.

**Table 3.** The band-gap values of pure and li-doped CuO.

| Sample | Pure-CuO | 3% Li–CuO | 6% Li–CuO | 9% Li–CuO | 12% Li–CuO | 15% Li–CuO |
|---|---|---|---|---|---|---|
| Band gap (eV) | 2.1722 | 2.2497 | 2.2549 | 2.5496 | 3.3048 | 3.5608 |

### *3.4. Photocatalytic Activity*

Nanostructured semiconductors present interesting photocatalytic properties [40–43]. ZnO and $TiO_2$ were the first nanostructured materials to be studied as photocatalysts against environmental pollutants [44,45]. CuO nanofilms have the capacity to remove contaminants of organic dyes as illustrated by the bleaching of aqueous methylene-blue (MB) solution under ultraviolet illumination.

The study of the catalytic properties consisted of introducing samples, both of pure CuO and doped with Li, into a solution of methylene blue (MB) that was subjected to UV irradiation. We recorded the decrease in the absorbance signal α after each 30 min of irradiation. The absorbance signal was composed of two peaks situated around 630 and 670 nm (Figure 7).

In Figure 7, we show the absorbance degradation of MB solution versus UV-irradiation time for pure CuO and for intermediate Li doping at 6 and 15%. From the curves, we observed that the MB solution was more degraded by the presence of Li-doped CuO than pure CuO. After 17 h of UV illumination, the absorbance decreased from 1.90 to 1.20 in the presence of 15% Li-doped CuO, while it has decreased to 1.30 in the case of pure CuO, which corresponded to an absorbance-signal decrease from 68 to 63% for both cases. In Figure 7d, the decrease in the absorbance signal with the increase in Li doping can be clearly observed.

We interpret these results in terms of electronic excitation processes caused by the ultraviolet irradiation and the differing morphology of the samples. When illuminated by UV light with an excitation energy (4.88 eV) greater than the band gap of Li–CuO (3.5608 eV for 15% Li–CuO), electron-hole pairs are created. Hydroxide groups created by the irradiation react with the photogenerated holes, producing O-H radicals. These radicals react with the MB solution dye and degrade it into non-toxic organic compounds.

As discussed in the previous paragraphs, the XRD and AFM results showed, for high Li doping (12–15%), a reduction in the CuO nanoparticle size. It is suggested that small CuO particles capture photons more efficiently, thereby generating electron-hole pairs in larger quantities and hence causing the more heavily doped CuO to exhibit a higher photocatalytic activity in the degradation of MB. As reported in our previous work [46], the photocatalytic phenomenon can be explained by the following steps:

(i) Step 1:

- During UV irradiation, electrons are extracted from the valence band to the conduction band; electron-hole pairs are then created.
- The created holes produce O-H radicals and peroxide groups ($O^{2-}$)
- The peroxides interact with the protons for forming $HO^{2-}$ and $H_2O^{2-}$ species.

(ii) Step 2:
The species interact with the solution and degrade it during UV irradiation. Step 1 and 2 are summarized by the following reaction:

$$CuO + h\nu\ (uv) \rightarrow CuO + e^- + h^+ \quad (6)$$

$$OH^- + h^+ \rightarrow OH^* \quad (7)$$

$$O_2 + e^- \rightarrow O^-{}_2 \quad (8)$$

$$O_2{}^- + H^+ \rightarrow HO_2 \quad (9)$$

$$2HO_2 \rightarrow H_2O_2 + O_2 \quad (10)$$

$$H_2O_2 + e^- \rightarrow OH^- + OH^- \quad (11)$$

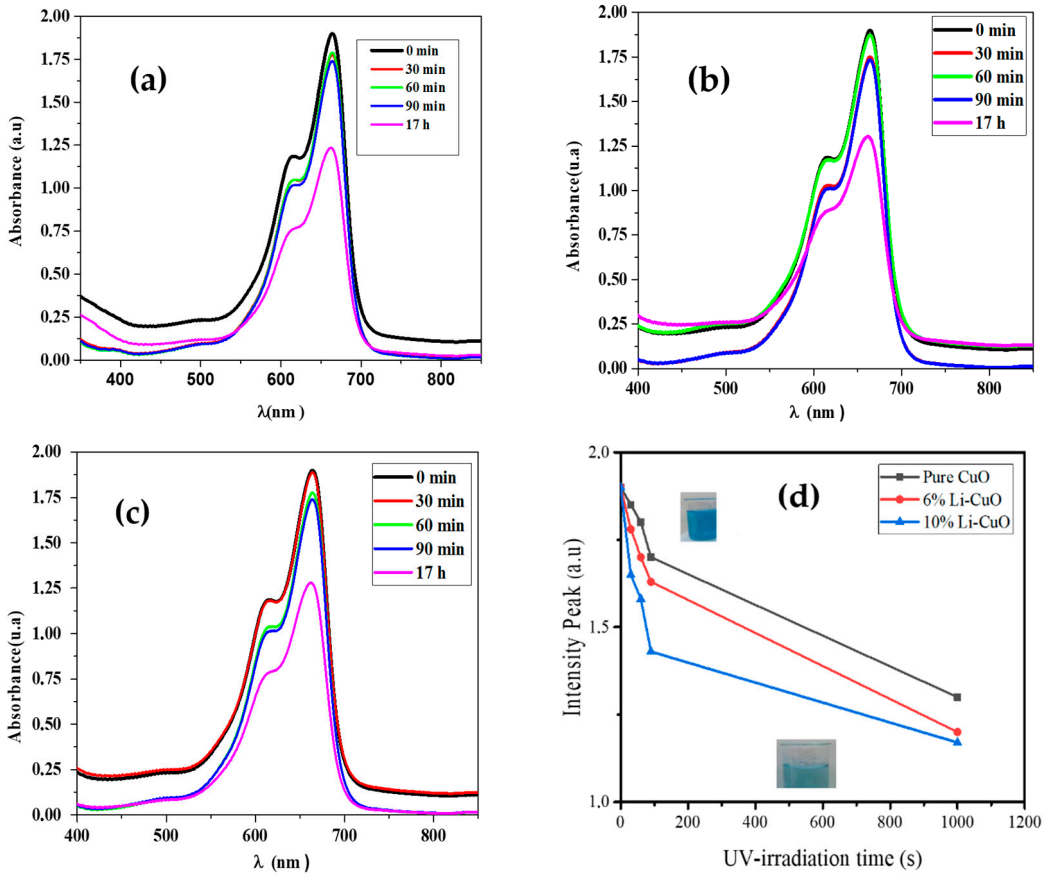


**Figure 7.** Effect of CuO nanofilms on the degradation of the MB solution under UV irradiation. (**a**) pure CuO, (**b**) 6% Li–CuO, (**c**) 15% Li–CuO. (**d**) Profile of absorbance intensity vs. irradiation time, the inserted beakers indicate the fading of MB solution during UV irradiation.

## 4. Conclusions

The present study led us to successfully synthesize pure and Li-doped copper-oxide films via the spray-pyrolysis technique. On the basis of the characterization results, we analyzed the effect of Li doping on the structural, morphological, optical and photocatalytic properties. CuO crystallization in monoclinic structure was revealed by XRD patterns. The surface morphology and its roughness were monitored by AFM microscope. The

inhomogeneous and textured CuO surface was improved by Li doping, which reduced grain sizes. The optical and photocatalytic properties were investigated in detail. The band gap of CuO films was in the range 2.1722–3.5608 eV for 15% from pure to 15% Li-doped CuO. The photo degradation of MB solution activated by Li–CuO particles allows displaying CuO as interesting material for eventual employ in environmental domain.

**Author Contributions:** M.G. proposed, designed the study and wrote the paper; S.A. and M.A.D. performed out the experiments and discussed the results, C.F. and D.T. contributed to the interpretations of the results and they take care of the article processing charge. In general all authors contributed to the preparation of this article. All authors have read and agreed to the published version of the manuscript.

**Funding:** This research is carried out jointly by the "Laboratoire des Sciences de la Matière Condensée (LSMC)" and the "Centre Interdisciplinaire de Nanosciences de Marseille" in the framework of a cooperation project. The authors would like to thank the French National Agency of Research (ANR) (project 'Nanoptix' # ANR-18-CE42-0016-02) for financial support.

**Institutional Review Board Statement:** Not applicable.

**Informed Consent Statement:** Not applicable.

**Data Availability Statement:** Data is contained within the article.

**Conflicts of Interest:** The authors declare no conflict of interest.

## References

1. Bielz, T.; Lorenz, H.; Jochum, W.; Kaindl, R.; Klauser, F.; Kloetzer, B.; Penner, S. Hydrogen on $In_2O_3$: Reducibility, bonding, defect formation, and reactivity. *J. Phys. Chem. C* **2010**, *114*, 9022. [CrossRef]
2. Golovanov, V.; Maki-Jaskari, M.A.; Rantala, T.T.; Korotcenkov, G.; Brinzari, V.; Cornet, A.; Morante, J. Experimental and theoretical studies of the indium oxide-based gas sensors deposited by spray pyrolysis. *Sens. Actuators B Chem.* **2005**, *106*, 563.
3. Fukano, T.; Motohiro, T. Low-temperature growth of highly crystallized transparent conductive fluorine-doped tin oxide films by intermittent spray pyrolysis deposition. *Sol. Energy Mater. Sol. Cells* **2004**, *82*, 567–575. [CrossRef]
4. Ouhaibi, A.; Ghamnia, M.; Dahamni, M.A.; Heresanu, V.; Fauquet, C.; Tonneau, D. The effect of Strontium doping on structural and morphological properties of ZnO nanofilms synthesized by ultrasonic spray pyrolysis method. *J. Sci. Adv. Mater. Devices* **2018**, *36*, 29–36. [CrossRef]
5. Hamzaoui, N.; Boukhachem, A.; Ghamnia, M.; Fauquet, C. Investigations of some physical properties of ZnO nanofilms synthesized by micro-droplets technique. *Results Phys.* **2017**, *7*, 1950–1958. [CrossRef]
6. Venkateswari, P.; Thirunavukkarasu, P.; Ramamurthy, M.; Balaji, M.; Chandrasekaran, J. Optimization and characterization of CuO thin films for P–N junction diode application by JNSP technique. *Optik* **2017**, *140*, 476–484. [CrossRef]
7. Khashan, K.S.; Hassan, A.I.; Addie, A.J. Characterization of CuO thin films deposition on porous silicon by spray pyrolysis. *Surf. Rev. Lett.* **2016**, *23*, 1650044. [CrossRef]
8. Cruccolini, A.; Narducci, R.; Palombari, R. Gas adsorption effects on surface conductivity of nonstoichiometric CuO. *Sens. Actuators B Chem.* **2004**, *98*, 227–232. [CrossRef]
9. Parvaz, M.; Khan, M.B.; Azam, A.; Khan, Z.H. Synthesis, characterization, and photocatalytic properties of CuO-$TiS_2$ nanocomposite. *Mater. Res. Express* **2019**, *6*, 125054. [CrossRef]
10. Umadevi, M.; Jeghatha Christy, J. Synthesis, characterization and photocatalytic activity of CuO nanoflowers. *Spectrochim. Acta Part A Mol. Biomol. Spectrosc.* **2013**, *109*, 133–137. [CrossRef]
11. Bayat, F.; Sheibani, S. Enhancement of photocatalytic activity of CuO-$Cu_2O$ heterostructures through the controlled content of $Cu_2O$. *Mater. Res. Bull.* **2022**, *145*, 111561. [CrossRef]
12. Dhanasekaran, V.; Mahalingam, T.; Ganesan, V. SEM and AFM studies of dip-coated CuO nanofilms. *Microsc. Res. Tech.* **2013**, *76*, 58–65. [CrossRef] [PubMed]
13. Fan, H.; Yang, L.; Hua, W.; Wu, X.; Wu, Z.; Xie, S.; Zou, B. Controlled synthesis of monodispersed CuO nanocrystals. *Nanotechnology* **2004**, *15*, 37–42. [CrossRef]
14. Marabelli, F.; Parravicini, G.B.; Salghetti-Drioli, F. Optical gap of CuO. *Phys. Rev. B* **1995**, *52*, 1433–1436. [CrossRef]
15. Tamm, A.; Tarre, A.; Verchenko, V.; Seemen, H.; Stern, R. Atomic Layer Deposition of Superconducting CuO Thin Films on Three-Dimensional Substrates. *Crystals* **2020**, *10*, 650. [CrossRef]
16. Phiwdanga, K.; Suphankij, S.; Mekprasarta, W.; Pecharapa, W. Synthesis of CuO Nanoparticles by Precipitation Method Using Different Precursors. *Energy Procedia* **2013**, *34*, 740–745. [CrossRef]
17. Kumar, S.K.; Murugesan, S.; Suresh, S.; Raj, S.P. Nanostructured CuO Thin Films Prepared through Sputtering for Solar Selective Absorbers. *J. Sol. Energy* **2013**, 147270.

18. Bollinger, A.T.; Wu, J.; Božović, I. Perspective: Rapid synthesis of complex oxides by combinatorial molecular beam epitaxy. *APL Mater.* **2016**, *4*, 053205. [CrossRef]
19. Ottosson, M.; Carlsson, J.O. Chemical vapour deposition of $Cu_2O$ and CuO from CuI and $O_2$ or $N_2O$. *Surf. Coat. Technol.* **1996**, *78*, 263–273. [CrossRef]
20. Nesa, M. Characterization of zinc doped copper oxide thin films synthesized by spray pyrolysis technique. Master's Thesis, Bangladesh University of Engineering and Technology, Dhaka, Bangladesh, 2016. Available online: http://lib.buet.ac.bd:8080/xmlui/handle/123456789/4510 (accessed on 17 April 2022).
21. Baturay, Ş.; Tombak, A.; Batibay, D.; Ocak, Y.S. n-Type conductivity of CuO thin films by metal doping. *Appl. Surf. Sci.* **2019**, *477*, 91–95. [CrossRef]
22. Chtouki, T.; Taboukhat, S.; Kavak, H.; Zawadzka, A.; Erguig, H.; Elidrissi, B.; Sahraoui, B. Characterization and third harmonic generation calculations of undoped and doped spin-coated multilayered CuO thin films. *J. Phys. Chem. Solids* **2019**, *124*, 60–66. [CrossRef]
23. Dahamni, M.A.; Ghamnia, M.; Naceri, S.E.; Fauquet, C.; Tonneau, D.; Pireaux, J.J.; Bouadi, A. Spray Pyrolysis Synthesis of Pure and Mg-doped Manganese Oxide Thin Films. *Coatings* **2021**, *11*, 598. [CrossRef]
24. Boulila, S.; Ghamnia, M.; Boukhachem, A.; Ouhaibi, A.; Chakhoum, M.A.; Fauquet, C.; Heresanu, V.; Tonneau, D. Photocatalytical properties of NiO nanofilms doped with Ba. *Phil. Mag. Letters.* **2020**, *110*, 283–293. [CrossRef]
25. Chakhoum, M.A.; Boukhachem, A.; Ghamnia, M.; Benameur, N.; Mehdi, N.; Raouadi, K.; Amlouk, M. An attempt to study (111) oriented NiO-like TCO thin films in terms of structural, optical properties and photocatalytic activities under strontium doping. *Spectrochim. Acta Part A* **2018**, *205*, 649–660. [CrossRef] [PubMed]
26. Diachenko, O.; Kováč, J., Jr.; Dobrozhan, O.; Novák, P.; Skriniarova, J.; Opanasyuk, A. Structural and Optical Properties of CuO Thin Films Synthesized Using Spray Pyrolysis Method. *Coatings* **2021**, *11*, 1392. [CrossRef]
27. Akgul, F.A.; Akgul, G.; Yildirim, N.; Unalan, H.E.; Turan, R. Influence of thermal annealing on microstructural, morphological, optical properties and surface electronic structure of copper oxide thin films. *Mater. Chem. Phys.* **2014**, *147*, 987–995. [CrossRef]
28. Momma, K.; Izumi, F. VESTA 3 for three-dimensional visualization of crystal, volumetric and morphology data. *J. Appl. Crystallogr.* **2011**, *44*, 1272–1276. [CrossRef]
29. Borchert, H.; Shevchenko, E.V.; Robert, A.; Mekis, I.; Kornowski, A.; Grubel, G.; Weller, H. Determination of nanocrystalsizes: Comparison of TEM; SAXS and XRD studies of highly monodisperse $CoPt_3$ particles. *Langmur* **2005**, *21*, 1931–1936. [CrossRef] [PubMed]
30. Muthukumaran, S.; Gopalakrishnan, R. Structural, FTIR and photoluminescence studies of Cu doped ZnO nanopowders by co-precipitation method. *Opt. Mater.* **2012**, *34*, 1946–1953. [CrossRef]
31. Chafi, F.Z.; Bahmad, L.; Hassanain, N.; Fares, B.; Laanab, L.; Mzerd, A. Characterization techniques of Fe-doped CuO thin films deposited by the Spray Pyrolysis method. *arXiv* **2004**, arXiv:1807.09697.
32. Abdel-Galil, A.; Moussa, N.L.; Yahia, I.S. Study on spray deposited Ni-doped CuO nanostructured thin films: Microstructural and optical behavior. *J. Mater. Sci. Mater. Electron.* **2022**, *33*, 4984–4999. [CrossRef]
33. Wu, J.; Hui, K.S.; Hui, K.N.; Li, L.; Chun, H.; Cho, Y.R. Characterization of Sn-Doped CuO Thin Films Prepared by Sol-Gel Method. *J. Mater. Sci. Mater. Electron.* **2016**, *27*, 1719–1724. [CrossRef]
34. Shariffudin, S.S.; Khalid, S.S.; Sahat, N.M.; Sarah, M.S.P.; Hashim, H. Preparation and Characterization of Nanostructured CuO Thin Films using Sol-gel Dip Coating. *IOP Conf. Ser. Mater. Sci. Eng.* **2015**, *99*, 012007. [CrossRef]
35. Moumen, A.; Hartiti, B.; Thevenin, P.; Siadat, M. Synthesis and characterization of CuO thin films grown by chemical spray pyrolysis. *Opt. Quant. Electron.* **2017**, *49*, 70. [CrossRef]
36. Tauc, J. *Amorphous and Liquid Semiconductors*; Springer: Berlin/Heidelberg, Germany, 1974; p. 159.
37. Singh, P.K.; Kumar, P.; Hussain, M.; Das, A.K.; Nayak, G.C. Synthesis and characterization of CuO nanoparticles using strong base electrolyte through electrochemical discharge process. *Bull. Mater. Sci.* **2016**, *39*, 469–478. [CrossRef]
38. Mukherjee, N.; Show, B.; Maji, S.K.; Madhu, U.; Bhar, S.K.; Mitra, B.C.; Khan, G.G.; Mondal, A. CuO nano-whiskers: Electrodeposition, Raman analysis, photoluminescence study and photocatalytic activity. *Mater. Lett.* **2011**, *65*, 3248–3250. [CrossRef]
39. Neeleshwar, S.; Chen, C.; Tsai, L.C.B.; Chen, Y.Y.; Shyu, S.G.; Seehra, M.S. Size-dependent properties of CdSe quantum dots. *Phys. Rev. B* **2005**, *71*, 201307. [CrossRef]
40. Saravanan, R.; Shankar, H.; Prakash, T.; Narayanan, V.; Stephen, A. ZnO/CdO composite nanorods for photocatalytic degradation of methylene blue under visible light. *Mater. Chem. Phys.* **2011**, *125*, 277–280. [CrossRef]
41. Vu, A.T.; Nguyen, Q.T.; Bui, T.H.L.; Tran, M.C.; Dang, T.P.; Tran, T.K.H. Synthesis and characterization of $TiO_2$ photocatalyst doped by transition metal ions ($Fe^{3+}$, $Cr^{3+}$ and $V^{5+}$). *Adv. Nat. Sci. Nanosci. Nanotechnol.* **2010**, *1*, 015009.
42. Zi-Qiang, X.; Hong, D.; Yan, L.; Hang, C. Al-doping effects on structure, electrical and optical properties of c-axis-orientated ZnO:Al thin films. *Mat. Sci. Semicon.* **2006**, *09*, 132–135. [CrossRef]
43. Kansal, S.K.; Singh, M.; Sud, D. Studies on photodegradation of two commercial dyes in aqueous phase using different photocatalysts. *J. Hazard. Mater.* **2007**, *141*, 581–590. [CrossRef] [PubMed]
44. Yeber, M.C.; Rodriguez, J.; Freer, J.; Duran, N.; Mansilla, H.D. Photocatalytic degradation of cellulose bleaching effluent by supported $TiO_2$ and ZnO. *Chemosphere* **2000**, *41*, 1193–1197. [CrossRef]

45. Atamnia, K.; Satha, H.; Bououdina, M. Synthesis and characterisation of $TiO_2$ nanostructures for photocatalytic applications. *Int. J. Nanopart.* **2018**, *10*, 225–243. [CrossRef]
46. Benameur, M.; Boukhachem, A.; Ghamnia, M.; Chakhoum, M.A.; Dahamni, M.A.; Fauquet, C. Investigation of Some Physical Properties of Cobalt Doped $MoO_3$ Nanofilms and Their Effects on the Degradation of the Methylene Blue Solution under UV Illumination. *Intern. J. Chem. Eng. Appl.* **2019**, *10*, 33–39. [CrossRef]